Available online at www.sciencedirect.com
SCIENCE DIRECT®
Journal of Solid State Chemistry 170 (2003) 48–57
JOURNAL OF SOLID STATE CHEMISTRY
http://elsevier.com/locate/jssc

REAu$_3$Al$_7$ (RE = rare earth): new ternary aluminides grown from aluminum flux

S.E. Latturner,[a] D. Bilc,[b] J.R. Ireland,[c] C.R. Kannewurf,[c] S.D. Mahanti,[b] and M.G. Kanatzidis[a,*]

[a] Department of Chemistry, Michigan State University, East Lansing, MI 48824-1322, USA
[b] Department of Physics, Michigan State University, East Lansing, MI 48824-1322, USA
[c] Department of Electrical and Computer Engineering, Northwestern University, Evanston, IL, USA

Received 22 May 2002; received in revised form 16 July 2002; accepted 5 August 2002

Abstract

A series of ternary aluminide intermetallics with a new structure type were formed from the reaction of gold and rare-earth metals in aluminum flux. The REAu$_3$Al$_7$ structure was obtained with all rare earths RE with the exception of La and Eu. These materials crystallize in the rhombohedral space group R-3c, with unit cell parameters $a = 8.0922(6)$ Å and $c = 21.066(2)$ Å for PrAu$_3$Al$_7$ as an example. The variation in cell edges with rare-earth size is regular with the exception of the Yb analogue. The possible mixed valency indicated by this result was confirmed by magnetic susceptibility measurements. Density functional theory-based band structure calculations on YbAu$_3$Al$_7$ indicate the ytterbium f-orbitals are located just below the Fermi level, further supporting the mixed valence description of this material.

1. Introduction

Aluminide intermetallics are ubiquitous. In commercial aluminum alloys (many of which also contain silicon), rare earths or transition metals are included to improve their properties, forming both known as well as yet unexplored multinary intermetallics within the aluminum matrix [1]. The study of possible multinary compounds formed during the alloying process is vital to understanding how to optimize the bulk material. Rare-earth aluminide binary and ternary compounds often possess complex structures and interesting magnetic and electronic behavior [2]. In our ongoing investigations of the use of aluminum flux as a growth medium for aluminide and silicide intermetallics, a number of new phases have been discovered. Examples of novel quaternary compounds containing a rare-earth element, a first or second row transition metal, aluminum, and silicon include $Sm_2Ni(Ni_xSi_{1-x})Al_6Si_4$ [3], $RE_8Ru_{12}Al_{49}Si_9(Al_xSi_{12-x})$ [4], and $RE_4Fe_{2+x}Al_{7-x}Si_8$. [5].

Recently, our explorations with third row transition metals revealed the intriguing finding that most of the flux-grown RE/Au/Al/Si structures contain building blocks of antifluorite-type AuAl$_2$. This is exemplified in the $Th_2[AuAl_2]_n(Au_xSi_{1-x})Si_2$ series of compounds [6]. To clarify the possible role of silicon in the formation/promotion of these moieties, similar reactions were carried out without including this element. In addition to the known BaAl$_4$-type ternaries REAuAl$_3$ [7], a new structure was found. The REAu$_3$Al$_7$ structure is very complex, shows little similarity to other known RE/Au/Al ternaries, and notably does not contain AuAl$_2$ slabs. Magnetic susceptibility studies and band structure calculations indicate that the ytterbium analogue is primarily in a 2+ state at room temperature, and in a mixed valent state at low temperatures.

2. Experimental procedure

2.1. Synthesis

The REAu$_3$Al$_7$ compounds were synthesized by combining the elements in a 1:2:15 molar ratio. In a nitrogen atmosphere glove box, 0.07–0.08 g rare-earth

*Corresponding author. Department of Chemistry, Michigan State University, East Lansing, MI 48824-1322, USA. Fax: +1-517-353-1793.
E-mail address: kanatzid@cem.msu.edu (M.G. Kanatzidis).

0022-4596/03/$ - see front matter © 2002 Elsevier Science (USA). All rights reserved.
PII: S0022-4596(02)00006-3

metal (Cerac, 99.99%), 0.197 g gold (1 ounce gold coin, 99.99%), and 0.203 g aluminum (Cerac, 99.99%) were combined in an aluminum crucible which was sealed in a fused silica tube under a vacuum of 10^{-4} Torr. The reaction vessel was heated to 1000°C in 12 h, held at this temperature for 15 h, then cooled to 860°C in a day. It was annealed at 860°C for 60 h, then cooled to room temperature in 3 days. The excess aluminum flux was removed by soaking the crucible in 5 M NaOH for 24 h.

To investigate other possible synthetic routes to this compound, reactions were also attempted with the oxides of Sm, Gd, Ho, Yb, and Lu (Sylvania, 99.9%), in a ratio of RE_2O_3/Au/Al of 0.5:2:25. The heating profile and isolation mechanism were identical to that described above for the non-oxide reactions. Arc melting was also explored, in particular for the La and Eu analogues which could not be isolated from the flux synthesis (vide infra). Pellets comprised of 0.5 mmol rare-earth metal, 1 mmol Au, and 3.5 mmol Al were pressed in a nitrogen-filled glove box, and then arc melted. The buttons were flipped and remelted four times to ensure homogeneity. Fragments of each were crushed and analyzed by powder X-ray diffraction; the remaining portions of pellet were annealed at 800°C for 1 week and then analyzed in the same manner.

Elemental analysis on the products was carried out using a JEOL JSM-35C scanning electron microscope with energy dispersive spectroscopy (EDS) capabilities. Ten to 20 crystals of each analogue were analyzed using a 20 kV accelerating voltage and an accumulation time of 50 s. In most cases the REAu$_3$Al$_7$ crystals were non-uniformly coated with a reflective reddish-purple film. EDS indicates this film is rich in rare earth and gold; it is possibly a binary such as RE_2Au$_7$, or a degradation product due to leaching of the aluminum in the compound by the NaOH solution. EDS on the interior of these samples indicates a stoichiometry of REAu$_3$Al$_6$. A slightly low reading for aluminum is not uncommon for this instrument.

2.2. X-ray diffraction

Single-crystal X-ray diffraction data for each compound were collected at room temperature on a Bruker AXS SMART CCD diffractometer. Data processing was then performed using the program SAINT; an absorption correction was applied to the data using the SADABS program [8]. The structure was solved using direct methods and refined with the SHELXTL package of programs [9]. The data collection parameters for three representative REAu$_3$Al$_7$ compounds are listed in Table 1; additional crystallographic refinement parameters can be found in the supporting material. Powder diffraction was carried out on the arc-melted pellets using an INEL powder diffractometer.

Table 1
Crystallographic collection parameters for three of the REAu$_3$Al$_7$ analogues

	PrAu$_3$Al$_7$	TmAu$_3$Al$_7$	YbAu$_3$Al$_7$
Formula weight (g/mol)	920.67	948.69	952.80
Space group	*R*-3*c*	*R*-3*c*	*R*-3*c*
a (Å)	8.0922(6)	7.998(1)	8.0272(9)
c (Å)	21.066(2)	20.922(4)	21.111(4)
V (Å^3)	1194.7(2)	1159.1(3)	1178.1(3)
d_{calc} (g/cm^3)	7.678	8.154	8.058
Temperature (K)	293	293	293
Radiation	Mo$K\alpha$	Mo$K\alpha$	Mo$K\alpha$
$2\theta_{max}$	74.64	55.98	55.98
Index ranges	$-11 \leqslant h \leqslant 13$	$-10 \leqslant h \leqslant 10$	$-10 \leqslant h \leqslant 10$
	$-11 \leqslant k \leqslant 13$	$-10 \leqslant k \leqslant 10$	$-10 \leqslant k \leqslant 10$
	$-33 \leqslant l \leqslant 35$	$-27 \leqslant l \leqslant 26$	$-27 \leqslant l \leqslant 27$
Reflections collected	3673	3428	3483
Unique data/parameters	662/20	314/20	321/20
μ (mm^{-1})	61.776	34.425	34.175
$R1$/w$R2$ [$I > 2\sigma(I)$]	0.0330/0.0765	0.0309/0.0725	0.0317/0.0783
$R1$/w$R2$ (all data)	0.0383/0.0783	0.0357/0.0746	0.0341/0.0791
Residual peaks (e/Å^3)	5.779/ − 7.043	5.694/ − 2.410	3.552/ − 3.002

$R1 = \sum(|F_o| - |F_c|)/\sum|F_o|$; w$R2 = [\sum[w(F_o^2 - F_c^2)^2]/\sum(w|F_o|^2)^2]^{1/2}$.

2.3. Magnetic susceptibility measurements

Magnetic susceptibility measurements were carried out with a Quantum Design MPMS SQUID magnetometer at temperatures between 3 and 300 K. For each analogue, EDS-analyzed crystals were ground into powder; this was sealed in kapton tape and placed into the magnetometer. Field-cooled and zero-field-cooled temperature dependence data were collected at 1000 G, and field dependence data were collected at 3 K. Magnetic susceptibility characteristics for the REAu$_3$Al$_7$ series are summarized in Table 6.

2.4. Band structure calculations

The electronic structure calculations for YbAu$_3$Al$_7$ was performed within density functional theory (DFT) using the self-consistent full potential linearized augmented plane wave (LAPW) [10] method implemented in WIEN 97 code [11]. For the exchange and correlation parts of the potential, the Perdew–Burke–Ernzerhof model was used, which incorporates a generalized gradient approximation (GGA) [12]. The atomic radii values (in atomic units 1 a.u. = 0.529 Å) used in the calculations are as follows: 2.5 a.u. for ytterbium, 2.5 a.u. for gold and 2.3 a.u. for aluminum. Self-consistent iterations were performed with 28 k points in the reduced Brillouin zone with a cutoff between valence and core states of −6.0 Ry; convergence was assumed when the total energy difference between cycles was within 0.0001 Ry. Scalar relativistic corrections were included and spin–orbit interaction was incorporated using a second variational procedure [13].

2.5. Transport measurements

Single crystals of $YbAu_3Al_7$ were embedded in thermoset and sanded down to remove the reddish-purple film and roughly shape the crystals into bars. Conductivity measurements were performed using the conventional four-probe technique [14]. Thermopower measurements were made using a slow AC technique as described elsewhere [15].

3. Results and discussion

3.1. Synthesis

Initial syntheses with *RE*: Au : Al reactant ratios of 1:1:10 produced low yields (less than 10% based on the amount of rare earth used) of $REAu_3Al_7$; more prevalent products included the $BaAl_4$-type $REAuAl_3$, and binary aluminides such as $REAl_3$. Increasing the amount of gold in the reaction (using a reactant ratio of 1:2:15) increased the yield of the title compound to 20–40%, with the yields for late rare earths being higher on average than those with early rare earths. This new ternary phase was not obtained from reactions with lanthanum and europium.

The $REAu_3Al_7$ materials can be distinguished from other byproducts not only due to the aforementioned purplish-red film, but also by their crystal habit. Binary aluminide compounds grow from the aluminum flux with distinctive crystal shapes such as hexagonal rods ($GdAl_3$) and cubes ($TmAl_2$); the ternary $BaAl_4$ analogues $REAuAl_3$ (especially prevalent for $RE = La$, Ce, Nd, and Eu) crystallize as large bevelled rectangular plates. The $REAu_3Al_7$ materials, on the other hand, form as glassy-looking silvery shards for the early rare earths (see Fig. 1a), and facetted blocks or conglomerates for the late rare earths. The purple film present in all cases (shown in Fig. 1c) can be scraped off or removed by sonication.

The facility of aluminum flux to reduce rare-earth oxide reagents has been utilized in the synthesis of compounds ranging from $Sm_2Ni(Ni_xSi_{1-x})Al_6Si_4$ to LaB_6 [2,16]. In this work, synthesis from the oxides was successful with Sm_2O_3, Gd_2O_3, and Ho_2O_3, but not with Yb_2O_3 or Lu_2O_3. The products of the successful reactions consisted of oxide powder, small gold crystals, and several large, facetted $REAu_3Al_7$ crystals, an example of which is shown in Fig. 1b. The crystals obtained from successful syntheses with oxide reagents are larger and more well-formed than those obtained from the use of rare-earth metal reactants. Again, these crystals were coated with a purplish-red film.

The arc-melting synthesis from a stoichiometric mixture of the elements was also successful in the formation of the $REAu_3Al_7$ phase. The powder diffraction pattern of the lutetium product indicates that the pellet was pure $LuAu_3Al_7$. The Sm, Gd, Ho, and Yb syntheses resulted in a mixture of phases. Predominant in the powder diffraction pattern of these pellets were the reflections from the $REAu_3Al_7$ phase, but the presence of small amounts of $AuAl_2$ (10–20%) and $REAuAl_3$ was also indicated. The opposite is true of the arc-melting attempts using lanthanum and europium; $AuAl_2$ and $REAuAl_3$ were the predominant products and there was no indication of $REAu_3Al_7$ in the powder patterns. Further evidence of the presence of $AuAl_2$ in the arc-melted pellets is the purple coloration of the La, Sm, Eu, Gd, and Ho products, caused by the $AuAl_2$ which is itself purple. The $LuAu_3Al_7$ pellet did not show such coloration. Annealing the pellets at 800°C for 1 week did not result in any significant change in the powder patterns.

The fact that this structure does not form with La and Eu may be due to size effects. Europium appears to favor the divalent state in many flux-grown aluminide intermetallics, and La^{3+} and Eu^{2+} have larger radii than the other rare-earth ions. These large cations may promote the growth of the $BaAl_4$-type $REAuAl_3$ (which is known for $RE = La$–Tb); indeed, these phases were

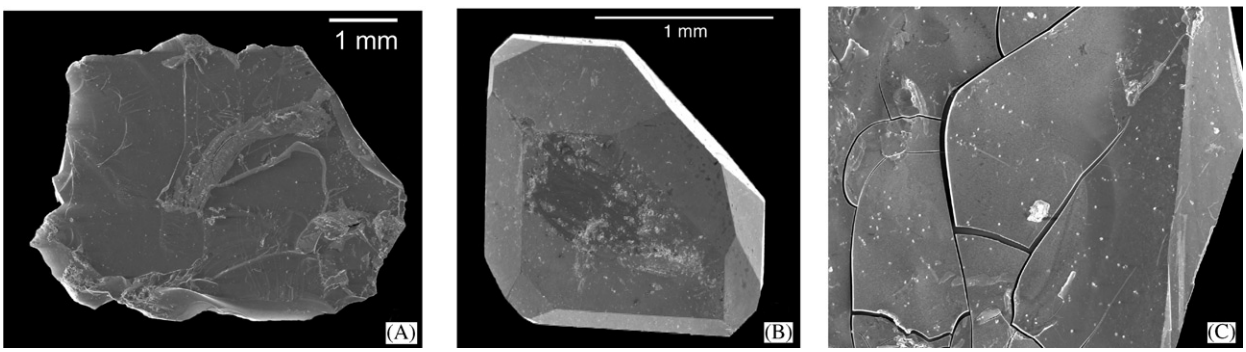

Fig. 1. Scanning electron micrographs of flux-grown $REAu_3Al_7$ crystals. (A) $YbAu_3Al_7$, (B) $HoAu_3Al_7$ product from oxide reaction and (C) a closeup of the reddish film on a crystal of $SmAu_3Al_7$.

the predominant product isolated from the La- and Eu-containing reactions. Additional evidence of the importance of cation size is the larger yields obtained for the later (smaller) rare earths.

3.2. Structure description

The REAu$_3$Al$_7$ compounds seem to possess a new structure type in the rhombohedral space group R-3c. The structure is depicted in Figs. 2 and 3 and the local environments for each crystallographic site are shown in Fig. 4; the atomic positions, anisotropic displacement parameters, and bond lengths for the YbAu$_3$Al$_7$ analogue are listed in Tables 2–4. The apparent complexity of the atomic arrangement in this structure type can be reduced if we consider the structure as a combination of layers. The gold atoms and Al(1) atoms form a monatomic layer, with each Al(1) atom being coordinated to three Au atoms in a trigonal planar fashion; this is shown in Fig. 3a. The Au–Al bond distance of 2.6069(6) Å is in agreement with that seen in other intermetallics containing these elements, although the planar configuration is unusual. The aluminum site in AlAu$_4$ is in an almost trigonal planar configuration, with the three nearest gold atoms at a distance of 2.592 Å and Au–Al–Au angles of 115.6°. However, there are other gold atoms within close bonding range (2.699 Å), so this aluminum site in AlAu$_4$ cannot be accurately described as trigonal [17].

Another feature of interest, the layer of aluminum triangles and rare-earth ions, is highlighted in Fig. 3c. Layers comprised of this Al triangle moiety interspersed with rare-earth ions have been observed in other intermetallic structures such as YNi$_3$Al$_9$, Y$_2$Co$_3$Al$_9$, and Gd$_3$Ru$_4$Al$_{12}$ [18]. However, in these compounds, the RE ions and Al triangles all lie in the same plane. In REAu$_3$Al$_7$, the RE ions are sandwiched in between two staggered layers of triangles roughly 1.2 Å apart. The Al–Al bond length in these triangles (2.831(5) Å) is relatively long compared to those seen in this structural motif in other intermetallics, which range from 2.64 to 2.75 Å. This may indicate a weakened interaction caused by withdrawal of bonding electrons by the gold atoms. It should be noted, however, that Al–Al bond lengths in other intermetallics can range up to 2.9–3.0 Å.

It is notable that this structure does not show similarities to other known RE/Au/Al ternary compounds. REAuAl$_3$ and REAu$_2$Al$_2$ both form in the tetragonal BaAl$_4$ structure (or ordered variants thereof) [7,19]; RE_3Au$_2$Al$_9$ forms in the α-La$_3$Al$_{11}$ structure type, which is related to the BaAl$_4$ type [20]. Despite the fact that the REAu$_3$Al$_7$ stoichiometry is the sum of REAuAl$_3$ and 2AuAl$_2$ (and the failed arc-melting reactions of LaAu$_3$Al$_7$ resulted in these two compounds in a 1:2 ratio), there is little evidence of antifluorite AuAl$_2$ slabs or BaAl$_4$-related motifs in the structure. Considering that several quaternary RE/Au/Al/Si compounds can be regarded as intergrowth structures

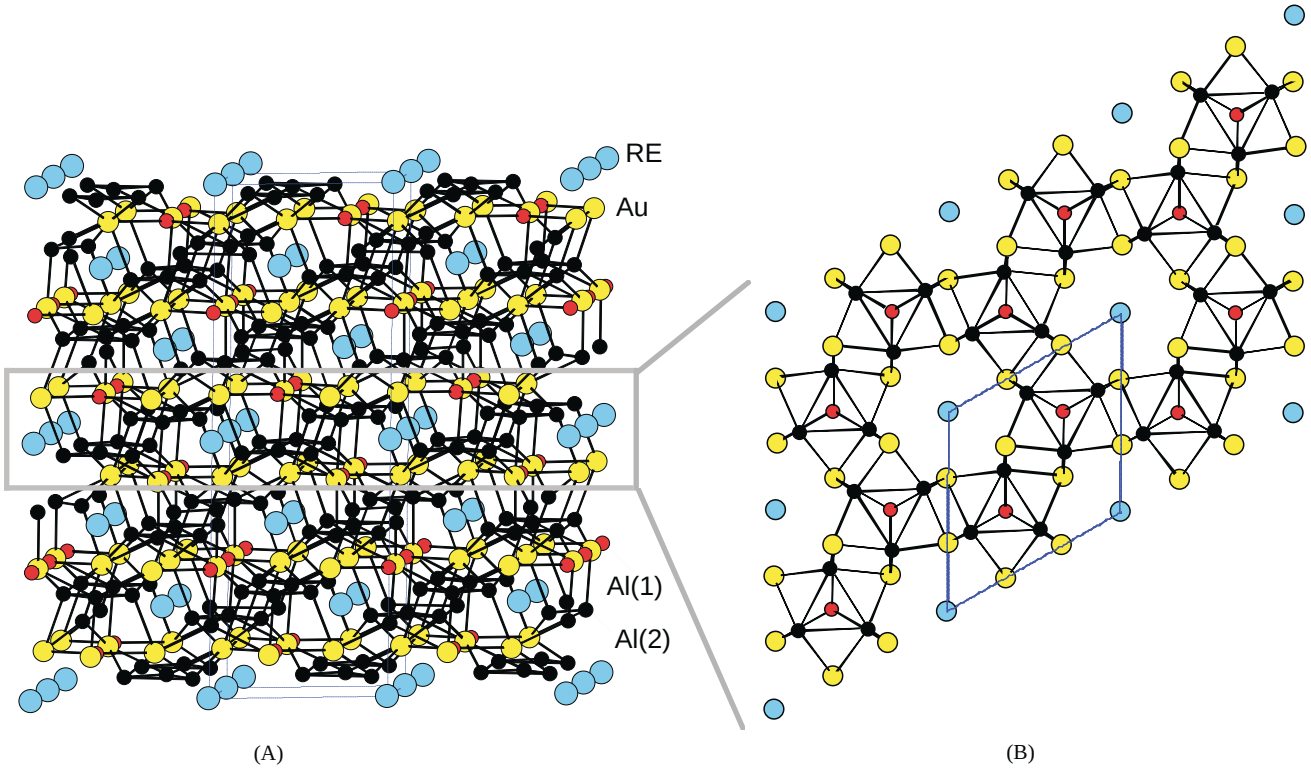

Fig. 2. (A) The structure of REAu$_3$Al$_7$ viewed down the a-axis and (B) a section of the structure, viewed down the c-axis.

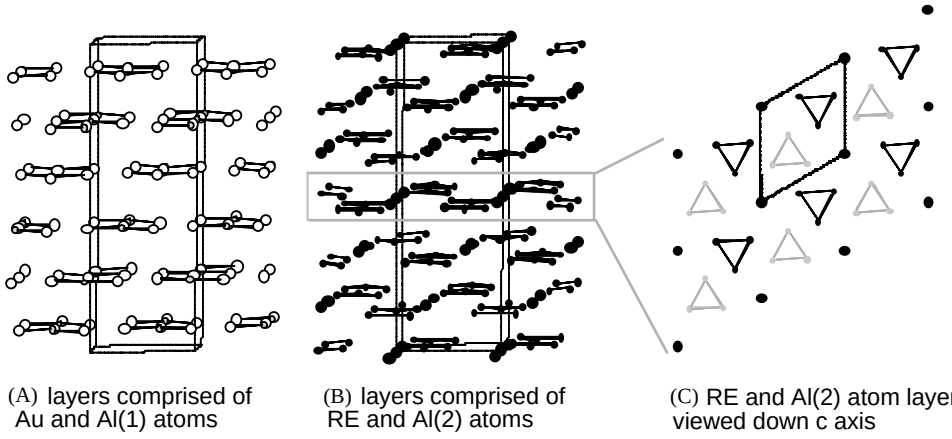

Fig. 3. Highlighted sections of the REAu$_3$Al$_7$ structure. (A) Layers comprised of Au and Al(1) atoms viewed down the a-axis, (B) layers comprised of the rare-earth atoms and the triangles of Al(2) atoms viewed down the a-axis and (C) a section of the structure viewed down the c-axis, showing the rare-earth atoms and the Al(2) atoms. The black Al(2) triangles are above the RE atom plane; the gray triangles are below the RE plane.

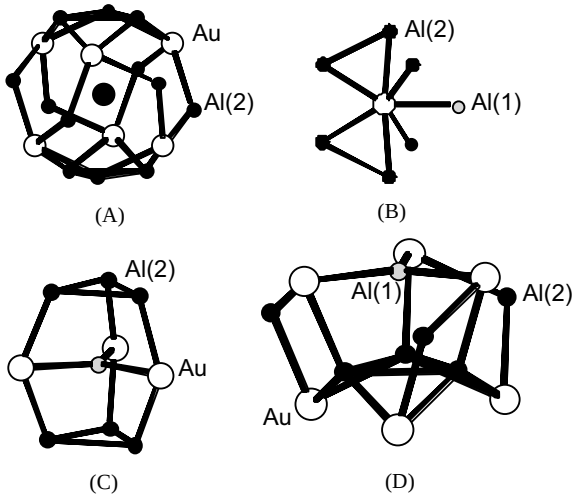

Fig. 4. Local coordination environment for sites in the REAu$_3$Al$_7$ structure. The coordination environment of (A) the rare-earth site, (B) the Au site, (C) the Al(1) site and (D) the Al(2) site.

Table 2
Atomic positions and equivalent isotropic displacement parameters (Å^2) for YbAu$_3$Al$_7$[a]

Atom	Wyckoff site	x	y	z	U_{eq}
Yb	6*b*	0	0	0	0.0062(4)
Au	18*e*	0.32476(6)	0	0.25	0.0069(3)
Al(1)	6*a*	0	0	0.25	0.009(1)
Al(2)	36*f*	0.0111(4)	0.2089(4)	0.1371(1)	0.0078(6)

[a] U_{eq} is defined as one-third of the trace of the orthogonalized U_{ij} tensor.

of AuAl$_2$ slabs and layers of other known structures such as BaAl$_4$ or CeNiSi$_2$, it is possible that the presence of silicon promotes the growth of the antifluorite AuAl$_2$ layer [6,21].

Table 3
Anisotropic thermal parameters (Å^2) for YbAu$_3$Al$_7$[a]

Atom	U_{11}	U_{22}	U_{33}	U_{23}	U_{13}	U_{12}
Yb	0.008(1)	0.008(1)	0.002(1)	0	0	0.004(1)
Au	0.009(1)	0.009(1)	0.002(1)	−0.001(1)	0.001(1)	0.004(1)
Al(1)	0.013(2)	0.013(2)	0.001(3)	0	0	0.007(1)
Al(2)	0.014(1)	0.010(1)	0.002(1)	−0.002(1)	−0.003(1)	0.008(1)

[a] The anisotropic factor exponent takes the form $-2\pi^2[h^2a^{*2}U_{11} + \cdots + 2hka^*b^*U_{12}]$.

Table 4
Bond lengths for YbAu$_3$Al$_7$

Bond	Length (Å)
Yb–Au	3.2317(4) × 6
Yb–Al(2)	3.324(3) × 6
	3.328(3) × 6
Au–Al(2)	2.576(2) × 2
	2.586(3) × 2
	2.659(3) × 2
Al(1)–Au	2.6069(6) × 3
Al(1)–Al(2)	2.890(3) × 6
Al(2)–Al(2)	2.831(5) × 2
	2.854(5) × 1
	2.868(5) × 1

The rare-earth ions in this structure are octahedrally coordinated to six gold atoms. Including the nearest aluminum atoms, it is apparent in Fig. 4a that the coordination geometry about the RE ions is roughly spherical. The variation of the unit cell parameters with rare earth is listed in Table 5 and plotted in Fig. 5. The decrease in both cell parameters and unit cell volume as the rare-earth radius gets smaller is regular, with the exception of ytterbium. This indicates that the ytterbium ions in YbAu$_3$Al$_7$ may be divalent, or in a fluctuating valence state. A valence bond sum calculation, based on

Table 5
Unit-cell parameters and fits for the RAu_3Al_7 compounds

Rare earth	a (Å)	c (Å)	Volume (Å^3)	$R1/wR2$
Ce	8.1050(7)	21.100(3)	1200.4(2)	0.0332/0.0768
Pr	8.0922(6)	21.066(2)	1194.66(18)	0.0330/0.0765
Nd	8.0892(6)	21.044(2)	1192.52(18)	0.0526/0.1379
Sm	8.0560(9)	20.974(3)	1178.8(3)	0.0411/0.1010
Gd	8.0384(6)	20.947(2)	1172.15(18)	0.0345/0.0830
Tb	8.0333(4)	20.9645(16)	1171.66(12)	0.0268/0.0623
Dy	8.0314(8)	20.952(3)	1170.4(2)	0.0391/0.1053
Ho	8.0056(16)	20.909(6)	1160.5(5)	0.0403/0.0935
Er	8.0058(6)	20.920(2)	1161.18(17)	0.0229/0.0551
Tm	7.9982(10)	20.922(4)	1159.1(3)	0.0309/0.0724
Yb	8.0272(9)	21.111(4)	1178.1(3)	0.0317/0.0783
Lu	7.9906(8)	20.913(3)	1156.4(2)	0.0272/0.0638

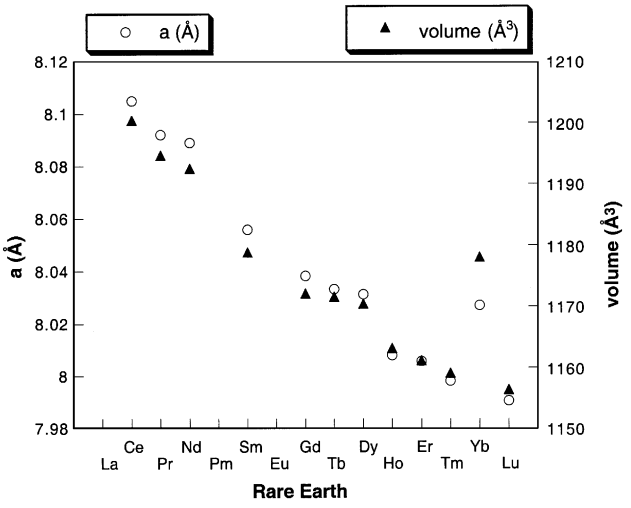

Fig. 5. The variation of RAu_3Al_7 unit cell parameter and volume across the rare-earth series.

the bond lengths between the ytterbium ion and its neighboring atoms (see Fig. 4a), indicates a valence of 1.92 at room temperature [22]. Further information about this is found in magnetic susceptibility measurements and band structure calculations.

3.3. Magnetic susceptibility studies

None of the RAu_3Al_7 compounds show any evidence of magnetic ordering down to 2 K. Because of the large separation of magnetic species in this structure (the closest RE–RE distance is 5.7–5.9 Å), the lack of magnetic transitions observed in the susceptibility data of these materials is not unexpected. The temperature dependence of the inverse susceptibility can be fit to the Curie–Weiss law for most of these compounds (see Fig. 6), resulting in the Weiss constants and magnetic moments per RE ion listed in Table 6. The Weiss constants are low, another indication of little to no interaction between the magnetic ions. The $SmAu_3Al_7$ analogue does not obey the Curie–Weiss law at high temperatures; this is likely due to the complex van Vleck paramagnetism often associated with samarium atoms [23].

The magnetic moments of the rare-earth ions are in agreement with the theoretical values, indicating that gold is in a diamagnetic state in these compounds. Diamagnetic late transition metals are a common feature of many ternary and quaternary aluminum-rich intermetallics [2–5]. Electrons are transferred from the electropositive rare earth and aluminum atoms to fill the d shell of the more electronegative transition metal, resulting in a diamagnetic atomic configuration.

The magnetization properties of the $REAu_3Al_7$ compounds vary from nearly linear M vs H behavior (for RE = Pr, Nd, Sm, Gd and Tb) to strongly plateaued data (for RE = Tm, Er). The data are shown in Fig. 7. The Er and Tm analogues show a saturation occurring at a field of 1.5 T; the moment per ion at this point is however only 70% of its maximum value, indicating the material may be in a metamagnetic state. A field higher than 5.5 T is necessary to achieve complete saturation of the magnetization. It is notable that these two samples are the only ones to have a positive Weiss constant, indicative of ferromagnetic coupling between spins. They also possess the smallest unit cells (with the exception of the non-magnetic Lu analogue). The RKKY coupling between magnetic moments in metallic samples, a function of the distance between the unpaired spins and the DOS at E_f, possesses an oscillating factor. Accordingly, as the distance between spins in a given structure is changed, the coupling can change from antiferromagnetic to ferromagnetic [24]. We speculate that this might be the reason for the switch from negative Weiss constants for RE = Ce–Dy (indicative of antiferromagnetic coupling) to the positive values of θ seen for Er and Tm.

The magnetic susceptibility behavior of $YbAu_3Al_7$ indicates that the ytterbium ions in this compound may be in a mixed valent state at low temperatures. The $1/\chi$ vs T data shown in Fig. 6 does not display Curie–Weiss behavior, instead indicating a very low and almost constant susceptibility at high temperatures, and an increasing of the magnetic moment per ion as the temperature drops below 150 K. This is evidence of a divalent Yb^{2+} state at high temperatures—resulting in Pauli paramagnetic behavior—changing to a mixed Yb^{2+}/Yb^{3+} state as the temperature is lowered. The previously mentioned anomalously large cell parameters (see Fig. 5) and the results of the valence bond sum calculation support the possibility of a divalent state at room temperature.

3.4. Transport properties

The low-temperature mixed valent state does not appear to have dramatic effects on the conductivity and

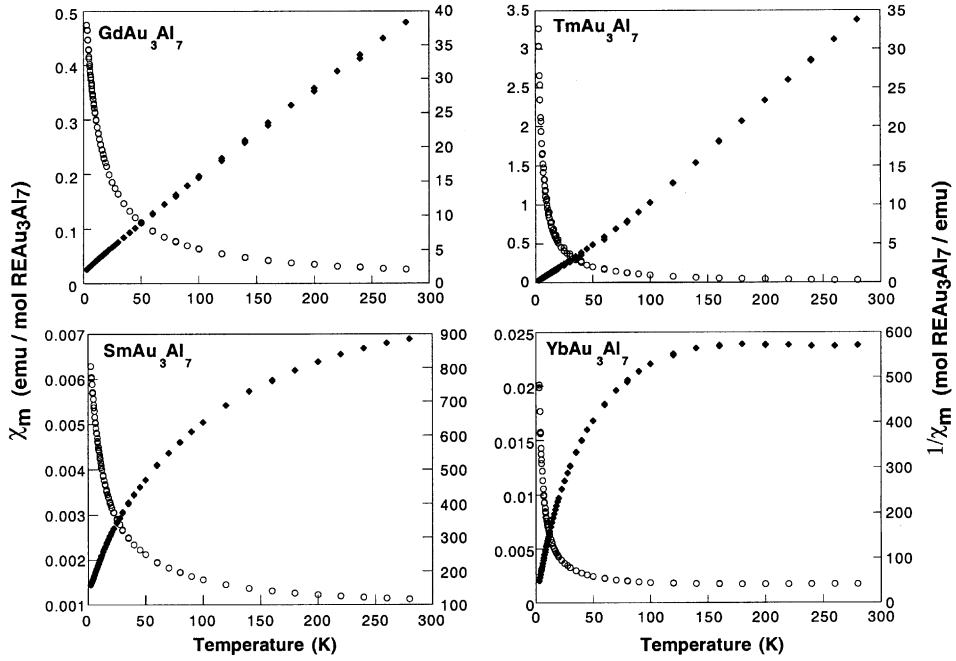

Fig. 6. Temperature dependence of the molar susceptibility χ_m (open circles) and inverse molar susceptibility $1/\chi_m$ (filled diamonds) for $GdAu_3Al_7$, $TmAu_3Al_7$, $SmAu_3Al_7$ and $YbAu_3Al_7$.

Table 6
Magnetic susceptibility data for $RE Au_3Al_7$ compounds

Rare earth	μ_{eff} (μ_B)	μ_{theo} (μ_B)[a]	θ (K)	Formal charge	Comments
Ce	2.56	2.54	−29.6	+3	
Pr	4.15	3.58	−13.8	+3	
Nd	3.79	3.62	−10.8	+3	
Sm		0.85		+3	Non CW behavior
Gd	7.90	7.94	−19.4	+3	
Tb	10.29	9.72	−2.5	+3	
Dy	9.98	10.65	−7.7	+3	
Ho	10.34	10.61	−2.9	+3	
Er	9.33	9.58	9.0	+3	Metamagnetic; $\mu_{eff} = 6.5\ \mu_B$
Tm	7.87	7.56	20.9	+3	Metamagnetic; $\mu_{eff} = 5.5\ \mu_B$
Yb		4.54		+2/ + 3	Mixed valent below 150 K

[a] Ref. [23].

thermopower of $YbAu_3Al_7$. The temperature dependence and magnitude of the conductivity (Fig. 8) are characteristic of a metal, rising from a room temperature value of 35,000 S/cm to a maximum of 167,000 S/cm at 4 K. The thermopower (not shown) is extremely low, below −1 μV/K at all temperatures. The small magnitude of the thermopower is also indicative of a metallic system; the negative sign suggests an n-type conductor.

3.5. Band structure calculations

Band structure studies were carried out on $YbAu_3Al_7$ to further investigate the mixed valency of this system. Immediately evident in the total density of states diagram (Fig. 9a) are the two sharp peaks, one just below the Fermi level, and one 1.5 eV below E_f. These are due to the narrow, non-disperse 4*f*-orbitals of Yb; the splitting of these orbitals results from spin–orbit coupling. Also evident in the total DOS are the bands derived from the gold *d*-orbitals, located between −4 and −7 eV, well below E_f. This indicates that the gold atoms in the structure possess a diamagnetic filled *d*-shell electronic configuration, in agreement with the magnetic susceptibility data for all the $RE Au_3Al_7$ compounds which show no paramagnetic contribution besides that of the rare-earth ions. Filled *d*-bands located several eV below E_f are a common feature of intermetallics formed from late transition metals combined with more electropositive elements.

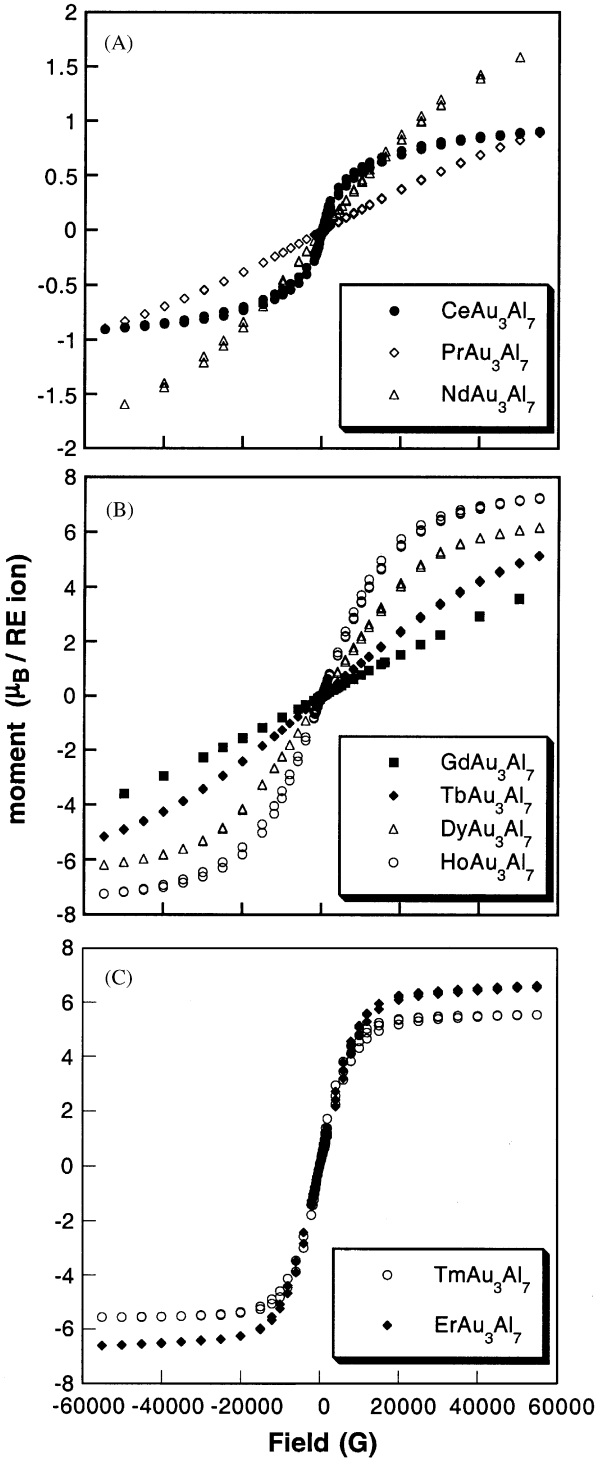

Fig. 7. Magnetization behavior at 3 K for the $RE Au_3Al_7$ compounds. (A) Data for the early rare-earth analogues (B) data for the Gd, Tb, Dy, and Ho analogues and (C) data for the Tm and Er analogues.

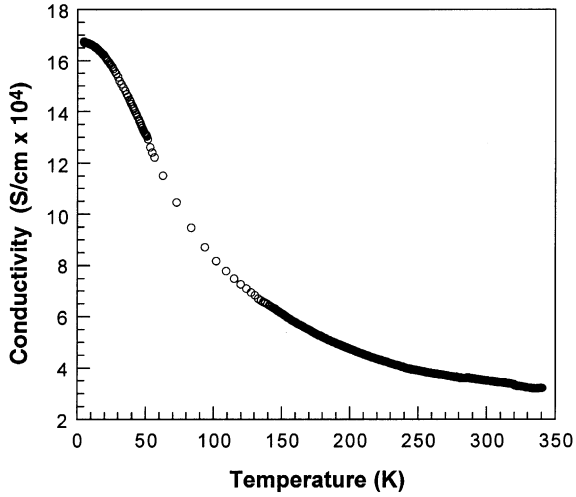

Fig. 8. Variable temperature single-crystal conductivity data for $YbAu_3Al_7$.

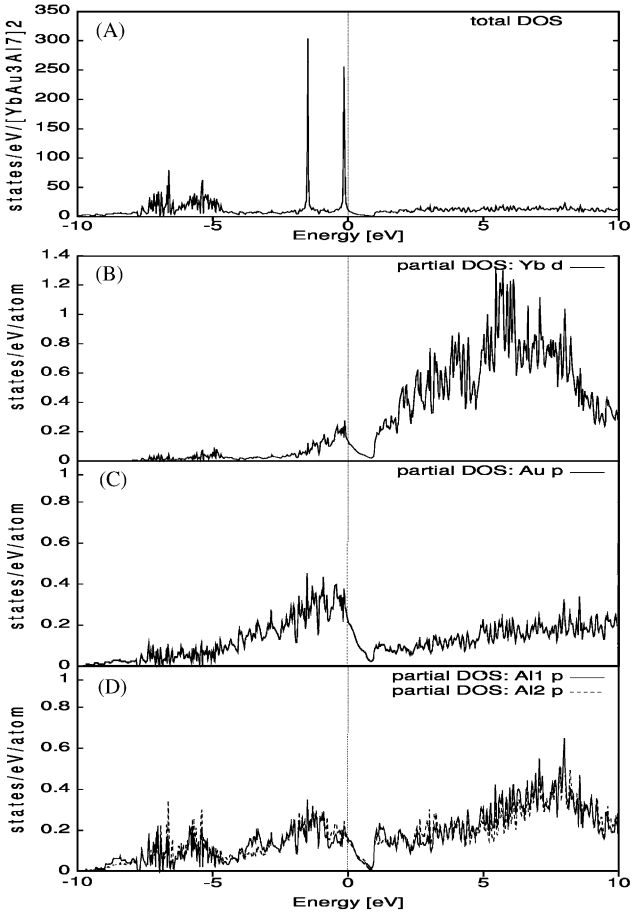

Fig. 9. Density of states diagrams for $YbAu_3Al_7$. The Fermi level is set at 0 eV and is indicated by the dotted line. (A) The total density of states. The two intense narrow peaks are due to the f-orbitals of Yb. (B) partial density of states of Yb d-orbitals, (C) partial density of states of Au p orbitals (D) partial density of states of Al(1) and Al(2) p orbitals.

In Fig. 9b, the bands derived from Yb 5d orbitals are shown. These range from -2 eV to around 10 eV, and overlap with the narrow 4f bands located just below E_f. This energy overlap between the rare earth f and d bands is a characteristic feature of mixed valent systems,

allowing the electronic configuration of the Yb ions to vary from the divalent $[Xe]4f^{14}$ to the trivalent $[Xe]4f^{13}$ state by transfer of an electron into the delocalized $5d$ band. Achieving the mixed valent state is contingent upon the relative energies and amount of overlap between the d band and the f levels, which can be modified by the application of pressure, addition of dopants, or (as is the case with $YbAu_3Al_7$) changing the temperature [25]. Below 150 K as the cell volume naturally contracts, a small effective pressure is applied so that the band overlap at E_f is optimized, allowing the ytterbium ions to exist as a mixture of Yb^{2+} and Yb^{3+}.

Also notable within the total DOS is a pseudogap at ca. 0.7 eV above E_f. This could possibly be due to hybridization of the Yb d-bands with s- or p-orbitals from gold or aluminum. In several intermetallic semiconductors such as FeSi, $RuAl_2$ and Fe_2VAl, the observed band gap at the Fermi level has been attributed to hybridization of the d-orbitals of the transition metal with the broad sp bands of the main group element [26]. In $YbAu_3Al_7$, the primary contribution to the density of states near the pseudogap is bands derived from the d orbitals of Yb and p orbitals of Au and Al. The partial densities of states of the latter atoms are shown in Fig. 9c and d. Comparison between these partial DOS diagrams indicate strong hybridization between Yb d-orbitals, Au p-orbitals, and the p-orbitals of Al(2). The local coordination environment of Yb is comprised of these particular atoms; interaction with their orbitals could result in the opening of a gap in the d-orbital manifold, producing a pseudogap in the density of states.

4. Conclusions

A new ternary intermetallic structure has been discovered with a complex atomic arrangement. This points out the utility of synthesis in aluminum flux for finding new compounds, even in systems which have been previously investigated by traditional methods. RAu_3Al_7 forms with all rare-earth metals except La and Eu. The structure bears little resemblance to other known RE/Au/Al compounds, and also does not possess the $AuAl_2$ slabs which characterize RE/Au/Al/Si systems. Magnetic susceptibility studies show no magnetic transitions in any analogue, and indicate that gold is diamagnetic in these compounds. The ytterbium analogue contains divalent ions at high temperature, becoming mixed valent below 150 K.

Supporting information available: Additional crystallographic data such as anisotropic thermal parameters and complete tables of bond distances and angles for all RAu_3Al_7 analogues are available. This information can be obtained from the Fachinformationszentrum Karlsruhe, 76344 Eggenstein-Leopoldshafen, Germany (Fax: (49) 7247-808-666; E-mail: crysdata@fiz.karlsruhe.de); the depository numbers for the 12 RAu_3Al_7 compounds are 39,1101–39,1112.

Acknowledgments

This work made use of the SEM facilities of the Center for Electron Optics at Michigan State University. Financial support from the Department of Energy (Grant DE-FG02-99ER45793) is gratefully acknowledged. Lu_2O_3 was kindly donated to us by Sylvania.

References

[1] (a) S. Suresh, A. Mortensen, A. Needleman, Fundamentals of Metal–Matrix Composites, Butterworth-Heinemann, Boston, 1993; (b) L.F. Mondolfo, Aluminum Alloys: Structure and Properties, Butterworths, Boston, 1979; (c) S. Gowri, F.H. Samuel, Metall. Mater. Trans. A25 (1994) 437–448.
[2] (a) K. H. J. Buschow, J. Alloys Compd. 193 (1993) 223; (b) CRC Handbook of Crystal Structures and Magnetic Properties of Rare Earth Intermetallics, CRC Press, Boca Raton, FI, 1994.
[3] X.Z. Chen, S. Sportouch, B. Sieve, P. Brazis, C.R. Kannewurf, J.A. Cowen, R. Patschke, M.G. Kanatzidis, Chem. Mater. 10 (1998) 3202–3211.
[4] B. Sieve, X.Z. Chen, R. Henning, P. Brazis, C.R. Kannewurf, J.A. Schultz, M.G. Kanatzidis, J. Am. Chem. Soc. 123 (2001) 7040–7047.
[5] B. Sieve, S. Sportouch, X.Z. Chen, J.A. Cowen, P. Brazis, C.R. Kannewurf, V. Papaefthymiou, M.G. Kanatzidis, Chem. Mater. 13 (2001) 273–283.
[6] S.E. Latturner, D. Bilc, S.D. Mahanti, M.G. Kanatzidis, Chem. Mater. 14 (2002) 1695–1705.
[7] F. Hulliger, J. Alloys Compd. 218 (1995) 255–258.
[8] SAINT, version 4, Siemens Analytical X-ray Instruments, Inc., Madison, WI; SADABS, G. M. Sheldrick, University of Göttingen, Göttingen, Germany.
[9] G. M. Sheldrick, 1995, SHELXTL. Structure Determination Programs, Version 5.0. Siemens Analytical X-ray Instruments, Inc. Madison, WI.
[10] (a) P. Hohenberg, W. Kohn, Phys. Rev. 136 (1964) B864; (b) W. Kohn, L. Sham, Phys. Rev. 140 (1965) A1133; (c) D. Singh, Planewaves, Pseudopotentials, and the LAPW Method, Kluwer Academic, Boston, 1994.
[11] P. Blaha, K. Schwarz, J. Luitz, WIEN97, a full potential linearized augmented planewave package for calculating crystal properties, Karlheinz Schwarz, Techn. Universität Wien, Austria, 1999.
[12] J.P. Perdew, K. Burke, M. Ernzerhof, Phys. Rev. Lett. 77 (1996) 3865.
[13] D.D. Koelling, B. Harmon, J. Phys. C 13 (1980) 6147.
[14] J.W. Lyding, H.O. Marcy, T.J. Marks, C.R. Kannewurf, IEEE Trans. Instrum. Meas. 37 (1988) 76–80.
[15] H.O. Marcy, T.J. Marks, C.R. Kannewurf, IEEE Trans. Instrum. Meas. 39 (1990) 756–760.
[16] P. Peshev, J. Solid State Chem. 133 (1997) 237–242.
[17] H. Buchler, K.J. Range, J. Less-Common Metals 161 (1990) 347–354.
[18] (a) Y. N. Grin, R. E. Gladyshevskii, O. M. Sichevich, V. E. Zavodnik, Y. P. Yarmolyuk, I. V. Rozhdestvenskaya, Sov. Phys. Crystallogr. 29 (1984) 528–530; (b) R. E. Gladyshevskii, K. Cenzual, H. D. Flack, E. Parthe, Acta Crystallogr. B 49 (1993) 468–474.

[19] F. Hulliger, H.U. Nissen, R. Wessicken, J. Alloys Compd. 206 (1994) 263–266.
[20] K.J. Nordell, G.J. Miller, Angew. Chem. Int. Ed. Engl. 36 (1997) 2008–2010.
[21] S. E. Latturner, M. G. Kanatzidis, in preparation.
[22] C. Hormillosa, S. Healy, Bond valence calculator (Version 2.0), Institute for Materials Research, McMaster University, Ontario, Canada, 1993.
[23] C. Kittel, Introduction to Solid State Physics, 6th Edition, John Wiley & Sons, New York, 1986, p. 405.
[24] K. Binder, K. Schroder, Phys. Rev. B 14 (1976) 2142.
[25] C.M. Varma, Rev. Mod. Phys. 48 (1976) 219–238.
[26] M. Weinert, R.E. Watson, Phys. Rev. B 58 (1998) 9732–9740.